

# Effect of metallicity on the gravitational-wave signal from the cosmological population of compact binary coalescences

I. Kowalska<sup>1</sup>, T. Regimbau<sup>2</sup>, T. Bulik<sup>1</sup>, M. Dominik<sup>1</sup> and K. Belczynski<sup>1</sup>

<sup>1</sup> *Warsaw University, Astronomical Observatory, Ujazdowskie 4, PL 00-478 Warsaw, Poland*

<sup>2</sup> *UMR ARTEMIS, CNRS, University of Nice Sophia-Antipolis,  
Observatoire de la Côte d'Azur, BP 4229, 06304, Nice Cedex 4, France*

(Dated: June 5, 2022)

Recent studies on stellar evolution have shown that the properties of compact objects strongly depend on metallicity of the environment in which they were formed. In this work, we study how the metallicity of the stellar population can affect unresolved gravitational waves background from extragalactic compact binaries. We obtain a suit of models of compact binaries using population synthesis code and estimate the gravitational wave background they produce. Our results show a double peaked structure for all considered models with the first peak between 30-100Hz caused by the binary black holes population and the second between 500-1000Hz corresponding to the double neutron stars population. We discuss the detectability of gravitational waves background with second (Advanced LIGO, Advanced Virgo) and third (Einstein Telescope) generation detectors.

PACS numbers:

## I. INTRODUCTION

The coalescence of two neutron stars (BNS), two black holes (BBH) or a neutron star and a black hole (NSBH), are the most promising sources of gravitational waves (GWs) for terrestrial detectors, due to the huge amount of energy emitted in the last phase of their inspiral trajectory, the merger and the ringdown. The coalescence occurs after two massive stars in a binary system have burned all their nuclear fuel, have evolved into red giants, and the cores have collapsed, possibly after supernova explosions, forming a bound system of two compact objects (neutron stars or black holes) inspiralling each other due to the emission of GWs. The number of massive systems that remain bounded after two supernova explosions (or prompt core-collapse) is uncertain, as well as the time to coalescence (the delay), or intrinsic parameters such as masses, spins, eccentricity, which depend on complicated evolution scenario involving common envelope and mass transfer. The distance probed with actual interferometers is about 30 Mpc for BNSs, but the next generation of detectors such as Ad LIGO/Virgo [1, 2], should be taking data with a sensitivity approximately 10 times greater, pushing the horizon up to about 450 Mpc. With the third generation interferometer Einstein Telescope (ET) [3], the horizon of compact binaries is expected to reach cosmological distances of  $z > 2 - 3$ , where it may become possible to study the evolution of the sources over redshift. Besides the emission produced by the coalescence of the nearest binary systems, the superposition of a large number of unresolved sources at high redshifts will produce a background of gravitational waves (see [7–12], for the most recent studies) that may dominate over the cosmological background in the range 10-1000 Hz where terrestrial detectors are the most sensitive. In the Laser Interferometer Space Antenna (LISA) band between  $10^{-4} - 0.1$  Hz [13], it is expected to remain after subtraction of the galactic foreground from white dwarf

binaries.

Recent studies have shown that the properties of the compact object binaries strongly depend on the metallicity of the stellar population. The formation rate of binaries containing black holes sharply increases with decreasing metallicity, as indicated both by observations [14, 15], and by binary population synthesis [16]. Moreover, it has been shown that at low metallicity the typical mass of a black holes increases [17]. While for the solar metallicity the maximum mass of a black hole is about  $10 - 15 M_{\odot}$ , for metallicity of about 10% solar value it rises to above  $30 M_{\odot}$ . The large redshift population of compact object merger originates in populations of star with various metallicities including very low ones. Thus investigation of the the gravitational wave background must take into account the effects of metallicity.

In this paper, we present a study this effect of the metallicity on the GW background from compact binaries (BNS, NSBH or BBH). In section II we describe how we use the simulation code **StarTrack** to derive sets of intrinsic parameters, in section III we discuss the calculation of the coalescence rate as a function of redshift, in section IV we derive the GW background and describe the numerical simulations, in section V we present our results, and finally in VI we summarize our main conclusions.

## II. SIMULATIONS OF A POPULATION OF COMPACT BINARIES WITH STARTRACK

For a simulated population of compact binaries, the intrinsic parameters, such as the masses  $m_1$  and  $m_2$  of the two components, the eccentricity  $e$ , the delay  $t_d$  are selected using the binary evolution code **StarTrack**. The masses of the compact objects are determined by the masses of the two progenitors and by mass loss and mass exchange during the common envelope phase (CE), when

the most massive star, already a neutron star or a black hole accretes mass from its companion, a red giant. The delay is the sum of the evolution time between the birth of the two massive progenitors and the formation of the compact binary ( $t_{evol}$ ), and the merging time, or the time it takes for the two stars to coalesce through the emission of GWs ( $t_{mr}$ ) [18].

$$t_d = t_{evol} + t_{mr}. \quad (1)$$

In order to model the population of compact object binaries we used the **StarTrack** population synthesis code [19] to perform a suite of Monte Carlo simulations of the stellar evolution of stars in environments of two typical metallicities:  $Z = Z_\odot = 0.02$  and  $Z = 10\% Z_\odot = 0.002$  [17]. In these calculations we employ the recent estimates of mass loss rates [16]. We calculate a population of 2 million massive binary stars, tracking the ensuing formation of relativistic binary compact objects: double neutron stars (BNS), double black hole binaries (BBH), and mixed systems (NSBH). Our modeling utilizes updated stellar and binary physics, including results from supernova simulations and compact object formation [5], incorporating elaborate mechanisms for treating stellar interactions like mass transfer episodes [22] or tidal synchronization and circularization [23]. We put special emphasis on the common envelope evolution phase [24], which is crucial for close double compact object formation as the attendant mass transfer allows for efficient hardening of the binary.

An important parameter describing the common envelope is the  $\lambda$  coefficient. It is a measure of how strongly the donor's envelope is bound to the core. We use the realistic calculations of the common envelope coefficient  $\lambda$  performed by [4], which now depends on the evolutionary stage of the donor, its mass at Zero Age Main Sequence (ZAMS), the mass of its envelope, and its radius. The orbital contraction occurring during the common envelope can be sufficiently efficient to cause the individual stars in the binary to coalesce and form a single highly rotating object, thereby aborting further binary evolution and preventing the formation of a double compact object. Because of significant radial expansion, stars crossing the Hertzsprung gap (HG) very frequently initiate a common envelope phase. HG stars do not have a clear entropy jump at the core-envelope transition [25]; if such a star overflows its Roche lobe and initiates a common envelope phase, the inspiral is expected to lead to a coalescence [26]. In particular, it has been estimated that for a solar metallicity environment (e.g., our Galaxy), properly accounting for the HG gap may lead to a reduction in the merger rates of BBH binaries by  $\sim 2 - 3$  orders of magnitude [27]. In contrast, in low metallicity environment this suppression is much less severe ( $\sim 1$  order of magnitude; [17]). The details of the common envelope phase are not yet fully understood, and thus in what follows we consider two set of models, one which does not take into account the suppression (optimistic models: marked with A), and set that assumes the maximum suppression

(pessimistic models: marked with B). In case of NSs we adopt natal kick distributions from observations of single Galactic pulsars [28] with  $\sigma = 265$  km/s. However for BHs we draw kicks from the same distribution but with the lower magnitude: inverse proportional to the amount of fall back expected at the BH formation [20]. In particular, for most massive BHs that form with the full fall back (the direct BH formation) the magnitude of natal kick is zero (more details on modeling can be found in [36]). Additionally we test one more set of models in which the magnitude of NS kicks is decreased by factor of 2:  $\sigma = 132.5$  km/s, as some observations and empirically based arguments seem to indicate that natal kicks in close binaries are lower than for single stars [29, 30]. The BH kicks are decreased in the similar fashion as in models with the full NS kicks. The standard value of  $\sigma$  parameter is denoted by K and smaller value by k. The detailed list of models considered in this paper is presented in Table I.

Detailed properties such as average total mass or average chirp mass are listed in Table II.

TABLE I: The list of models of stellar evolution used in the paper. Sigma is a parameter of the natal kick distribution, while HG specifies whether we have optimistic (+) or pessimistic (-) model. For more details see text.

Model	Metallicity	$\sigma$ [km s $^{-1}$ ]	HG
AZK	$Z_\odot$	265.0	+
BZK	$Z_\odot$	265.0	-
AZk	$Z_\odot$	132.5	+
BZk	$Z_\odot$	132.5	-
AzK	$10\% Z_\odot$	265.0	+
BzK	$10\% Z_\odot$	265.0	-
Azk	$10\% Z_\odot$	132.5	+
Bzk	$10\% Z_\odot$	132.5	-

### III. THE COSMIC COALESCENCE RATE

We assume that for each category of binaries ( $k = \text{BNS, NSBH, BBH}$ ), the coalescence rate tracks the star formation rate albeit with some delay  $t_d$  from formation of the massive binary to final merger :

$$\dot{\rho}_c^k(z) = A^k \int \frac{\dot{\rho}_*(z_f)}{1 + z_f} P(t_d) dt_d, \quad (2)$$

where  $\dot{\rho}_*$  is the star formation rate in  $M_\odot \text{Mpc}^3 \text{yr}^{-1}$ ,  $A^k$  is the mass fraction of the progenitors in  $M_\odot^{-1}$  (see Appendix for more details),  $P^k(t_d)$  is the probability distribution of the delay  $t_d$ ,  $z_f$  is the redshift at which the progenitor binary forms, and  $z$  is the redshift at which the two compact objects coalesce. The factor  $(1 + z_f)^{-1}$  converts the rate in the source frame into a rate in the observer frame. The redshifts  $z_f$  and  $z$  are related by the

TABLE II: Statistical properties of compact binaries used in the simulations. For each model we listed average total mass of a binary, average chirp mass, and average frequency at last stable orbit.

Model	$\langle M_{tot} \rangle$ [M $_{\odot}$ ]	$\langle M_{chirp} \rangle$ [M $_{\odot}$ ]	$\langle f_{lso} \rangle$ [Hz]
BNS			
BZK	2.43	1.05	1811.26
BZk	2.43	1.05	1809.39
BzK	2.49	1.08	1768.23
Bzk	2.49	1.08	1770.95
AZK	2.43	1.05	1809.71
AZk	2.43	1.06	1809.53
AzK	2.51	1.09	1756.74
Azk	2.49	1.08	1765.63
NSBH			
BZK	9.85	3.13	448.39
BZk	9.49	3.04	469.29
BzK	12.45	3.21	371.55
Bzk	11.77	3.10	390.27
AZK	9.91	3.17	444.89
AZk	9.85	3.13	449.20
AzK	11.66	3.17	398.82
Azk	11.47	3.11	404.41
BBH			
BZK	15.60	6.76	282.59
BZk	15.49	6.72	285.12
BzK	22.41	9.54	215.14
Bzk	22.26	9.50	214.34
AZK	15.56	6.74	283.66
AZk	15.33	6.64	288.50
AzK	30.31	13.08	188.09
Azk	28.51	12.29	198.89

delay time  $t_d$  which is the difference in lookback times between  $z_f$  and  $z$ :

$$t_d = \frac{1}{H_0} \int_z^{z_f} \frac{dz'}{(1+z')E(\Omega, z')} . \quad (3)$$

The coalescence rate per redshift bin is then given by:

$$\frac{dR^k}{dz}(z) = \dot{\rho}_c(z) \frac{dV}{dz}(z) , \quad (4)$$

The co-moving volume element :

$$\frac{dV}{dz}(z) = 4\pi \frac{c}{H_0} \frac{r(z)^2}{E(\Omega, z)} , \quad (5)$$

where

$$r(z) = \frac{c}{H_0} \int_0^z \frac{dz'}{E(\Omega, z')} , \quad (6)$$

and

$$E(\Omega, z) = \sqrt{\Omega_\Lambda + \Omega_m(1+z)^3} . \quad (7)$$

In these simulations, we used the cosmological model derived from 7 years of WMAP observations [6] and assumed a flat Universe with  $\Omega_m = 0.27$ ,  $\Omega_\Lambda = 0.73$  and Hubble parameter  $H_0 = 70.3 \text{ km s}^{-1} \text{ Mpc}^{-1}$ . Following [7, 8], we used the SFR of [31], which is derived from measurements of the galaxy luminosity function in the UV (SDSS, GALEX, COMBO17) and FIR wavelengths (Spitzer Space Telescope), and is normalized by the Super Kamiokande limit on the electron antineutrino flux from past core-collapse supernovas. This model is expected to be quite accurate up to  $z \sim 2$ , with very tight constraints at redshifts  $z < 1$  (to within 30 – 50%). In order to account for uncertainties in the SFR, we also considered the model presented by [32]. However, as we'll see in the next section, and as already noticed by [7], the uncertainties on the star formation history affecting essentially redshift  $z > 2$  where sources don't contribute significantly to the integrated signal, our final results are not expected to vary by more than a factor 2, depending on the choice of the SFR. The final rate is just the sum of the rates from the different categories :

$$\frac{dR}{dz}(z) = \frac{dR^{\text{BNS}}}{dz}(z) + \frac{dR^{\text{NSBH}}}{dz}(z) + \frac{dR^{\text{BBH}}}{dz}(z) . \quad (8)$$

TABLE III: Total coalescence rate of all compact binaries per year is presented in second column. In the last three columns we show contribution of each type of compact binaries to the total coalescence rate.

Model	rate [yr $^{-1}$ ]	rate <sub>BNS</sub> [%]	rate <sub>NSBH</sub> [%]	rate <sub>BBH</sub> [%]
BZK	154 929	84.78	2.09	13.13
BZk	157 559	86.28	0.94	12.78
BzK	319 304	10.70	11.50	77.80
Bzk	364 564	7.59	15.90	76.51
AZK	622 572	71.62	3.70	24.69
AZk	784 762	74.30	2.54	23.16
AzK	1 606 240	10.62	3.56	85.82
Azk	1 842 390	9.73	4.55	85.72

#### IV. THE GW BACKGROUND

The superposition of the GW signal from sources at all redshifts create a background, whose spectrum is usually characterized by the dimensionless energy density parameter [33]:

$$\Omega_{gw}(f) = \frac{1}{\rho_c} \frac{d\rho_{gw}}{d \ln f} , \quad (9)$$

where  $\rho_{gw}$  is the gravitational energy density and  $\rho_c = \frac{3c^2 H_0^2}{8\pi G}$  the critical energy density needed to make the Universe flat today.

The GW spectrum from the population of extra-galactic binaries is given by the expression:

$$\Omega_{gw}(f) = \frac{1}{\rho_c c} f F(f). \quad (10)$$

where  $F(f)$  is the total flux and  $f$  is observed frequency.

In this paper, we estimate the total flux (in  $\text{erg Hz}^{-1}$ ) as the sum of the individual contributions, whose redshift and masses are given by the **StarTrack** simulations:

$$F(f) = T^{-1} \sum_{k=1}^N \frac{1}{4\pi d_L^2(z^k)} \frac{dE_{gw}}{df}(f, f_{lso}^k, \mathcal{M}_c^k, z^k), \quad (11)$$

where  $\frac{dE_{gw}}{df}(f, f_{lso}^k, \mathcal{M}_c^k, z^k)$  is the spectral energy density (in  $\text{ergHz}^{-1}\text{s}^{-1}$ ) averaged over orientation for a binary at redshift  $z^k$ , with chirp mass  $\mathcal{M}_c^k$  and frequency  $f_{lso} = c^3/(6\sqrt{6}\pi GM)$  at the last stable orbit (ISCO). In the quadrupole approximation, and assuming circular orbit:

$$\begin{aligned} \frac{dE_{gw}}{df}(f, f_{lso}^k, \mathcal{M}_c^k, z^k) = & \quad (12) \\ \frac{(G\pi)^{2/3}(\mathcal{M}_c^k(1+z^k))^{5/3}}{3} f^{-1/3}, & \\ \text{for } f < f_{lso}^k/(1+z^k), & \end{aligned}$$

where  $\mathcal{M}_c^k(1+z^k)$  is the observed (redshifted) chirp mass and  $f_{lso}^k/(1+z^k)$  is the observed frequency at the ISCO.  $N$  is the number of sources produced by **StarTrack** and corresponds to the number of coalescences in  $T = 1 \text{ yr}$ . The normalization factor  $T^{-1}$  assures that the flux has the correct dimension.

For each category of binary, we can use the following approximate analytical expression, which involves the rates derived in the previous section and average quantities :

$$F^j(f) \simeq \int_0^{z_{max}} \frac{1}{4\pi d_L^2(z)} \frac{dE_{gw}}{df}(f, \bar{f}_{lso}^j, \bar{\mathcal{M}}_c^j, z) \frac{dR^j}{dz}(z) dz, \quad (13)$$

where  $j = \text{BNS, NSBH or BBH}$ ,  $\bar{f}_{lso}^j$  is the average frequency at ISCO and  $\bar{\mathcal{M}}_c^j$  the average chirp mass of the population. This expression provides a very estimate of the background in the low frequency region (before the ISCO), and in the case the chirp mass and the delay distributions show little correlation.

Inserting Eq. 13 in Eq. 10, we obtain for the contribution to  $\Omega_{gw}$  of each type of binaries :

$$\begin{aligned} \Omega_{gw}^j(f) \simeq & \quad \frac{2\pi^{2/3}G^{5/3}}{9c^3H_0^2} (\bar{\mathcal{M}}_c^j)^{5/3} f^{2/3} \quad (14) \\ & \int_0^{z_{sup}^j(f)} \frac{dR^j}{dz}(z) \frac{dz}{r(z)(1+z)^{1/3}} dz. \end{aligned}$$

with

$$z_{sup}^j(f) = \begin{cases} z_{max} & \text{if } f < \bar{f}_{lso}^j/(1+z_{max}) \\ (\bar{f}_{lso}^j/f) - 1 & \text{otherwise} \end{cases} \quad (15)$$

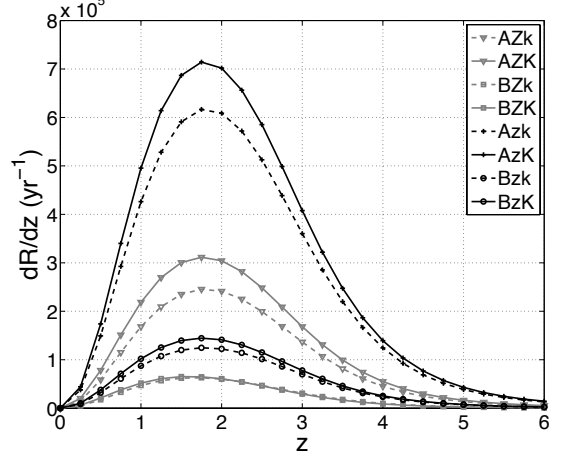


FIG. 1: Rate of compact binary coalescences as a function of the redshift for the different values of the metallicity and for the different models Table I: AZK (gray continuous line with triangle symbol), AZk (gray dashed line with triangle symbol), BZK (gray continuous line with square symbol), BZk (gray dashed line with square symbol), AzK (black continuous line with cross symbol), Azk (black dashed line with cross symbol), BzK (black continuous line with circle symbol), Bzk (black dashed line with circle symbol). Black lines correspond to low metallicity and gray lines to high (solar) metallicity, continuous lines to low kick velocity and dashed lines to high kick velocity.

## V. RESULTS AND DISCUSSION

We present the dependence of compact object binary coalescence rate on the redshift in Figure 1. The shape of the distributions is very similar for all the models, as the distribution of the delay does not show noticeable differences from one model to the other, except from differences in the minimal value of the delay, which is much smaller than the Hubble time and doesn't affect significantly the final distribution. The coalescence rate peaks at around  $z \sim 1.7$ , and is then shifted toward lower redshift compared to the star formation rate whose maximal is rather at  $z \sim 2$ . The normalization, on the other hand, changes, as it is linked to the compact object formation rate specific for each model. Typically models A (optimistic) correspond to higher rates than models B (pessimistic), and models with low metallicity lead to higher overall rates than the models with high metallicity. The value of the kick velocity has very small influence on the coalescence rate. We must note that the models presented are calculated for a few particulars population synthesis models. Thus the absolute normalization of the results is uncertain, just as any rate calculation in the literature. A detailed discussion of the expected rates based on the **StarTrack** population synthesis models will be published separately by [36].

The resulting gravitational wave background spectrum

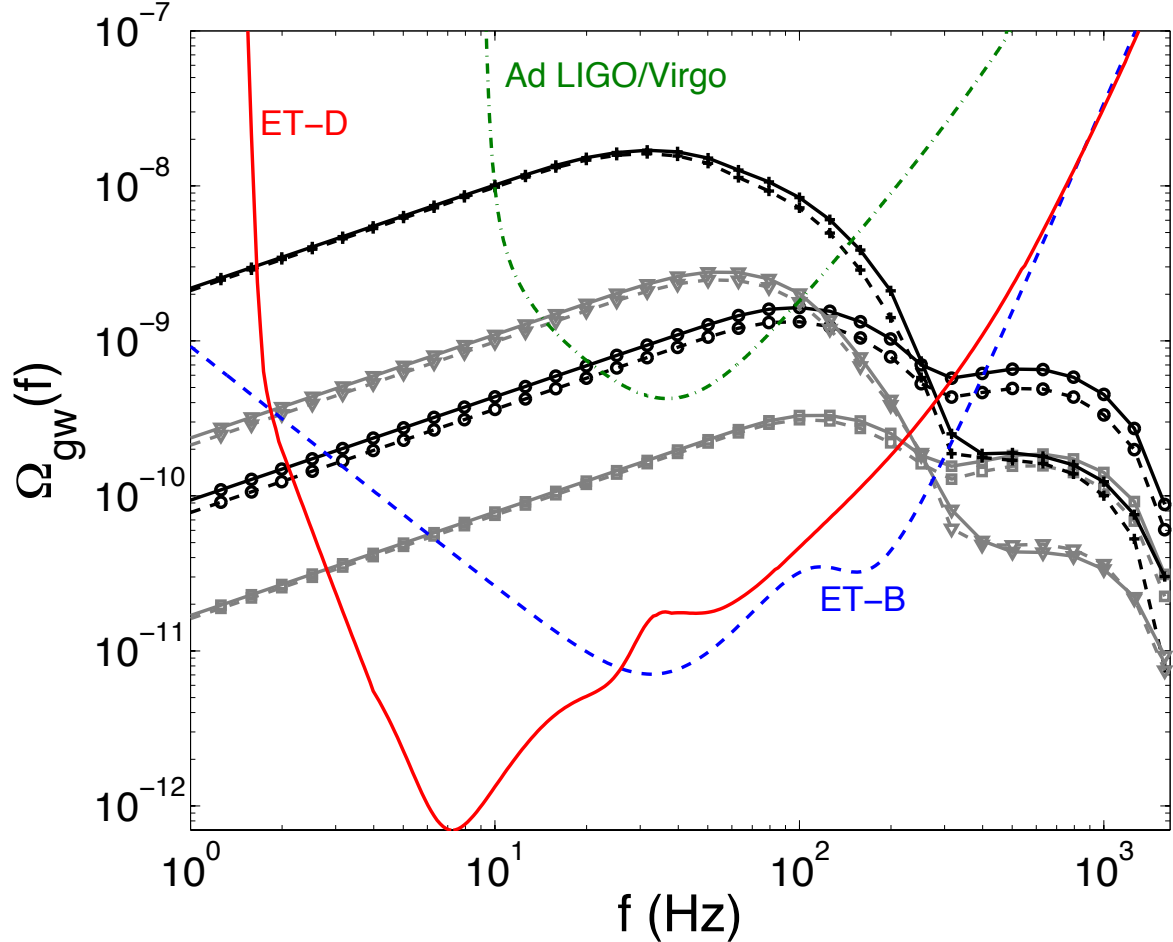


FIG. 2: Energy density parameter of the background produced by the coalescence of compact binaries for the different values of the metallicity and for the different models considered in this paper: AZK (gray continuous line with triangle symbol), AZK (gray dashed line with triangle symbol), BZK (gray continuous line with square symbol), BZk (gray dashed line with square symbol), AzK (black continuous line with cross symbol), Azk (black dashed line with cross symbol), BzK (black continuous line with circle symbol), and Bzk (black dashed line with circle symbol). Black lines correspond to low metallicity and gray lines to high (solar) metallicity, continuous lines to low kick velocity and dashed lines to high kick velocity. The sensitivity of ET-B, ET-D and Advanced LIGO/Virgo are also shown for comparison purpose.

for the models BZk and Bzk are presented in Figure 3 with the individual contributions of each type of binaries shown separately. For each contribution, the density parameter evolves as  $\Omega_{gw} \sim f^{2/3}$  at lower frequencies (see Eq. 15), reaches a maximum at a frequency corresponding roughly to the last stable orbit at  $z \sim 1.5$  where the coalescence rate is maximal, and decreases sharply until the cutoff at  $f_{LSO}$ . The more massive the population is, the smaller the peak frequency and  $f_{LSO}$  are. The amplitude of the background scales up with the rate and the average chirp mass (see Eq. 15) and is larger for the BBH background than for the NSBH and BNS contributions by 1 – 3 orders of magnitude. Consequently, at low frequencies, the background is dominated by the signal

from BBH. After the BBH peak, the spectrum decreases dramatically, and we recover the BNS contribution at high frequencies. The population of NSBH contributes very little to the total background since it is masked by the BBH signal at low frequencies, and, even in the low metallicity case BzK, where it is above the BNS contribution, its maximum is buried in the decrease after the BBH peak.

The spectra for the different models of Table I are presented together in Figure 2. All the models show the same characteristic two-peaked structure described previously, with a first peak between 30 – 100 Hz, corresponding to the population of BBH, and a second peak at about 500 – 1000 Hz corresponding to the population

of BNS. The first thing to notice is that the kicks do not affect the shape of the GW background spectrum significantly. This can be expected as the kicks affect neither the chirp mass distribution nor the delay time distribution. The effect of the choice of the model A or B (with different treatment of the CE with HG donor) affects mainly the normalization of the spectrum. The change of the metallicity of the underlying population changes both the level and the shape of the spectrum. The lower metallicity population contains more high mass BHs and therefore the low frequency peak shifts to the lower frequencies. The position of the high frequency peak remains unchanged, as the NS masses do not depend on the stellar metallicity. The level of the spectrum shifts up with decreasing metallicity. This is due to increase of the formation rate of compact object binaries with the decreasing metallicity.

The gravitational wave background as presented in Figure 2 is maximal in the frequency band of terrestrial interferometers (1 Hz-10 kHz), and could be accessible by the next generations of detectors. The standard detection method of cross correlation between two detectors gives a signal-to-noise ratio (SNR):

$$SNR = \frac{3H_0^2}{4\pi^2} \sqrt{2T} \left[ \int_0^\infty df \frac{\gamma^2(f) \Omega_{gw}^2(f)}{f^6 P_1(f) P_2(f)} \right]^{1/2} \quad (16)$$

where  $\gamma$  is the overlap reduction function characterizing the loss in sensitivity due to the separation and the relative orientation of the detectors, normalized so that it is one for L-shaped co-aligned and co-located detectors, and  $P_1$  and  $P_2$  are the strain noise power spectral densities of the two detectors.

In this paper we consider 1) a pair of co-aligned and co-located Advanced (second generation detectors such as the LIGO Hanford pair in the US. A similar sensitivity can be obtained by combining the future network of detector pairs worldwide (LIGO Hanford and LIGO Livingston in the US, Virgo in Italy, GEO in Germany, IndIGO in India, KAGRA in Japan), the number of pairs balancing the loss in sensitivity due to their separation and relative orientation ([8], Mandic private communication). 2) a pair of V-shaped detectors (an angle of  $\pi/3$  between the two arms) separated by an angle of  $2\pi/3$ , with the sensitivity of the third generation triangle detector ET. We use two models for the noise, ET-B [34] which is about ten times better than the sensitivity of Advanced LIGO/Virgo with a low frequency cutoff at 1 – 3 Hz, and ET-D [35] with a significant improvement at frequencies below 30 Hz.

In Fig. 4, we show the cumulative SNR as a function of the frequency for Advanced and ET detectors for the model BZk (considering other models or a simple power law  $\Omega_{gw} \sim f^{2/3}$  do not change the results significantly). As one can see, most of the SNR comes from the power-law low frequency region, where the BBH contribution dominates.

The SNR is reported in Table IV for all the models,

assuming an integration time of 1 yr. Models with low metallicities should be detected by Advanced detectors with  $SNR \sim 7 - 57$  so about 2 – 20 times larger than the detection threshold of  $SNR = 2.5$  (for a false alarm rate and false dismissal rate of 10% [33]). Models with high metallicity are accessible at the detection threshold for model A but are out of reach for model B by a factor of a few. With Einstein Telescope, all the models should be detectable with very high signal-to-noise ratio, between  $SNR \sim 39 - 4155$  for ET-B and  $102 - 14485$  for ET-D.

TABLE IV: For the different models presented in Table I, signal-to-noise ratio obtained by cross-correlating two co-aligned and co-located Advanced detectors or a pair of two ET detectors with the sensitivity ET-B or ET-D.

Model	Ad CC	ET-B	ET-D
BZK	0.6	41	107
BZk	0.5	39	102
BzK	7.9	568	1567
Bzk	6.8	490	1350
AZK	3.2	234	614
AZk	2.7	195	512
AzK	57	4155	14485
Azk	52	3750	13466

Another very promising detection method that have been tested in the context of the ET Mock Data Challenge [12] for the population of BNS is to look at the residual of the null stream which contains no GW signal and arises from the sum of the three ET detectors. In this case, it should be possible to identify the double peak structure, which would provide valuable information about the mass distributions of the different types of binaries.

## VI. CONCLUSIONS

The main result of this paper is the demonstration of a double peak structure in the gravitational wave background spectrum at high frequencies. The low frequency peak at 10-100 Hz arises due to a large population of BBH binaries predicted by the current population synthesis models. Such structure has already been pointed one for a single case by [10], where he used the BBH rate observational estimate by [14]. We show that the double peak structure appears also for the solar metallicity stellar population, and the low frequency peak increases for the low metallicity population. This results are in agreement with the estimate of detectability of the gravitational wave background by [11]. Thus detection of the gravitational wave background will impose significant constraints on the mass spectrum and formation rates of the compact object binaries.

In the paper we have only calculated the contribution of the inspiral signal to the gravitational wave back-

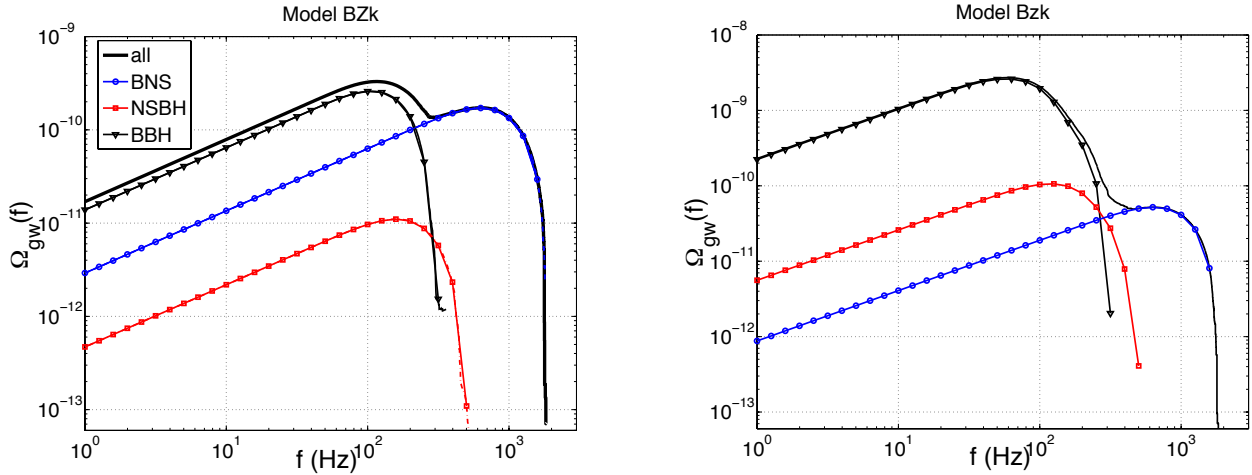


FIG. 3: Energy density parameter of the background produced by the coalescence of the different type of binaries : two neutron stars (blue continuous line with circle symbol), a neutron star and a black hole (red continuous line with square symbol) two black holes (black continuous line with triangle symbol), for model B with low kick and with metallicities  $Z = Z_{\odot}$  (top) and  $Z = 10\% Z_{\odot}$  (bottom) . The tick black line correspond to the sum of all the contributions.

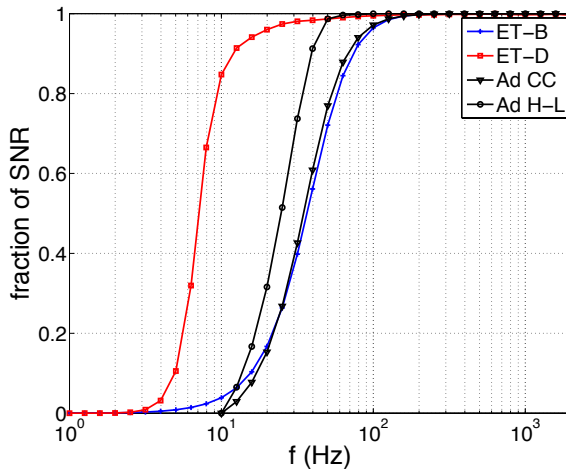


FIG. 4: Contribution to the  $SNR$  of frequencies  $< f$ , for co-aligned and co-located Advanced detectors, separated Advanced detectors (the LIGO Hanford/Livingston pair), and the third generation Einstein Telescope (ET-B and ET-D)

ground. In general, also the merger and ringdown should be taken into account. The addition of these two contributions carries quite a lot of uncertainty due to lack of precise knowledge of the amount of energy emitted in these phases. [9] have calculated the contributions of these two phases to the gravitational background spectrum from BBH coalescences. They have shown that the addition of these two phases causes extension of the peak of the spectrum to higher frequencies. Thus the double peaked structure of the spectrum will remain after addition of merger and ringdown.

#### Acknowledgements

This work was supported by the FOCUS 4/2007 Program of Foundation for Polish Science, the Polish grants N N203 302835, N N203 511238, N N203 404939, GR 4071, N/ST9/03171, DPN/N176/VIRGO/2009, and the Associated European Laboratory “Astrophysics Poland-France”

---

[1] <http://www.ligo.caltech.edu/docs/M/M060056-10.pdf>.  
[2] <https://wwwcascina.virgo.infn.it/advirgo/docs.html>  
[3] Punturo M. et al., 2010, *Class. Quantum Grav.* 27 194002  
[4] Xu, X.-J. and Li, X.-D., 2010, *ApJ*, 716, 114  
[5] Fryer, C. L., Belczynski, K., Wiktorowicz, G. et al., 2012, *ApJ*, 749, 91  
[6] Komatsu E. et al., *ApJ Suppl.*, 2011, 192:18  
[7] Regimbau T., 2011, *RAA*, 11, 369; arXiv:1101.2762 (re-

vised version)  
[8] Zhu X.-J. et al., arXiv:1104.3565.  
[9] Marassi S. et al., 2011 arXiv:1104.2044.  
[10] Rosado P., 2011, arXiv:1106.5795.  
[11] Wu C., Mandic V., Regimbau T., 2011, arXiv:1112.1898  
[12] Regimbau T. et al., 2012, arXiv:1201.3563  
[13] Bender P. L. and the LISA Study Team, *Laser Interferometer Space Antenna for the Detection of Gravitational Waves, Pre-Phase A Report*, MPQ233 (Max-

Plank-Institüt für Quantenoptik, Garching) (1998)

[14] Bulik T., Belczynski K, and A. Prestwich, 2011, ApJ, 730, 140.

[15] Bulik T. and Belczynski K., 2010, Memorie della Societa Astronomica Italiana, 81, 302.

[16] Belczynski K., Bulik T., Fryer C. L. et al., 2010b, ApJ, 714, 1217

[17] Belczynski K., Dominik M., Bulik T. et al., 2010a, ApJ, 715, L138

[18] Peters P. C. and Mathews J., 1963, Phys. Rev., 131, 435

[19] Belczynski K., Kalogera V. and Bulik T., 2002b, ApJ, 572, 407

[20] Fryer C. L. and Kalogera V., 2001, ApJ, 554, 548

[21] Timmes F. X., Woosley S. E. and Weaver T. A., 1996, ApJ, 457, 834

[22] Belczynski K. et al., 2008, ApJS, 174, 223

[23] Hut P., 1981, A&A, 99, 126

[24] Webbink R. F., 1984, ApJ, 277, 355

[25] Ivanova N. and Taam R. E., 2004, ApJ, 601, 1058

[26] Taam R. E. and Sandquist E. L., 2000, ARA&A, 38, 113

[27] Belczynski K., Taam R. E., Kalogera V. et al., 2007, ApJ, 662, 504

[28] Hobbs G., Lorimer D. R., Lyne A. G. et al., 2005, MNRAS, 360, 974

[29] Dessart L., Burrows A., Ott C. D. et al., 2006, ApJ, 644, 1063

[30] Kitaura F. S., Janka H. and Hillebrandt, 2006, A&A, 450, 345

[31] Hopkins A. M. and Beacom J., 2006, ApJ, 651, 142

[32] Springel V. and Hernquist L., 2003, MNRAS, 339, 312

[33] Allen B. and Romano J., 1999, Phys. Rev. D, 59, 102001.

[34] S. Hild et al., 2008, arXiv:0810.0604v2.

[35] S. Hild et al., 2011, Class. Quant. Grav., 28, 094013.

[36] Dominik M., Belczynski K., Fryer C., et al., arXiv:1202.4901

[37] Salpeter E. E., 1955, ApJ, 121, 161

### Appendix A: Normalization of the cosmic coalescence rate

To normalize coalescence rate, we need to take into account various factors. First of all, our simulations can not be treated as a complete sample of realistic stars. We do not cover whole parameter space, in particular the mass range is narrower than in reality. Also, not all stars that are born in binaries will end up as a compact binaries. Most of them will not survive the common envelope stage.

Coalescence rate for one particular binary  $i$  is given by following formula:

$$\dot{\rho}_{c,i}(z) = \frac{1}{N_{sim}} n_{bin} f_s, \quad (\text{A1})$$

where  $N_{sim}$  is the total number of binaries that started their evolution on ZAMS in the **StarTrack** code. In our case that number is  $2 \times 10^6$ ,  $n_{bin}$  is the number density of stars in binaries,  $f_s$  = is the fraction of simulated binaries.

In the Universe not only binaries are formed. Total Star Formation Rate ( $\dot{\rho}_*$ ) is a sum of a contribution from

binaries and single stars.

$$\dot{\rho}_* = \dot{\rho}_{*bin} + \dot{\rho}_{*sin} [M_\odot \text{Mpc}^{-3} \text{yr}^{-1}]. \quad (\text{A2})$$

Number density will be defined as:

$$n_k = \frac{\dot{\rho}_{*k}}{\langle M_k \rangle} [\text{Mpc}^{-3} \text{yr}^{-1}], \quad (\text{A3})$$

where  $k = \text{"bin"}$  or  $\text{"sin"}$  and  $\langle M_k \rangle$  is the average mass of a star in a binary, if  $k = \text{bin}$ , or a single star, if  $k = \text{sin}$ .

Another important parameter is binary fraction, which is defined as a fraction between number of binary systems and total number of all systems (binary and single).

$$f_b = \frac{N_{bin}}{N_{bin} + N_{sin}} = \frac{0.5 n_{bin}}{0.5 n_{bin} + n_{sin}}, \quad (\text{A4})$$

where  $N_{bin}$  is the number of binaries, not the stars, so we need factor of 0.5 in the second par of the equation. We set binary fraction to be  $f_b = 0.5$ , as it is for a current stellar populations.

By transforming Eq. A4 we obtain number density of a single stars:

$$n_{sin} = \frac{1}{2} n_{bin} \frac{1 - f_b}{f_b}, \quad (\text{A5})$$

then, combing eq. A2 and A3 we have number density of stars in binaries:

$$n_{bin} = \dot{\rho}_* \frac{2}{\frac{1-f_b}{f_b} \langle M_{sin} \rangle + 2 \langle M_{bin} \rangle}, \quad (\text{A6})$$

$$n'_{bin} = \frac{2}{\frac{1-f_b}{f_b} \langle M_{sin} \rangle + 2 \langle M_{bin} \rangle}. \quad (\text{A7})$$

As a next step we need to compute average masses of single star and of those that are components of a binary. We used Initial Mass Function (IMF) proposed by Salpeter [37] and flat mass ratio distribution.

$$\Psi(M) = KM^{-2.7}, \quad (\text{A8})$$

$$\Phi(q) = 2q, \quad (\text{A9})$$

where  $K^{-1} = \int_{M_{min}}^{M_{max}} M^{-2.7} dM$ ,  $M_{min} = 0.08M_\odot$ ,  $M_{max} = 150M_\odot$ .

Using IMF we can compute average masses of a single stars and components of a binaries.

$$\langle M_{sin} \rangle = \int_{M_{min}}^{M_{max}} M \Psi(M) dM, \quad (\text{A10})$$

$$\langle M_{bin} \rangle = \frac{1}{2} \int_{M_{min}}^{M_{max}} M \Psi(M) dM \int_0^1 dq (1+q) \Phi(q), \quad (\text{A11})$$

The form of  $f_s$  is a consequence of a specific way of drawing masses of the components in **StarTrack**. First mass of the primary is drawing from Salpeter distribution with  $M_{min,sim} = 5M_\odot$  and  $M_{max,sim} = M_{max}$ . Then, the mass of the secondary is determined by mass ratio, which is taken from a flat distribution. Mass of the second component has to be greater than  $3M_\odot$ . Fraction of simulated stars can be express by:

$$f_s = \frac{\int_{M_{min,sim}}^{M_{max}} dM \Psi(M) \int_{q_{min}(M)}^1 dq \Phi(q)}{\int_{M_{min}}^{M_{max}} dM \Psi(M) \int_0^1 dq \Phi(q)} \quad (\text{A12})$$

where  $q_{min}(M) = \frac{3}{M}$ .

Normalization  $A^k$  (k=BNS, NSBH or BBH) can be define as:

$$A^k = \frac{N^k}{N_{sim}} n'_{bin} f_s [M_\odot^{-1}] \quad (\text{A13})$$

$N^k$  is the number of k-type binaries in our simulations. Detailed list of that values for all models is presented in Table V

TABLE V: Number of binaries of each type produced in all models.

Model	$N^{BNS}$	$N^{NSBH}$	$N^{BBH}$
BZK	1618	43	395
BZk	1994	56	441
BzK	509	475	2873
Bzk	464	885	3175
AZK	4940	326	1721
AZk	6710	404	2164
AzK	1698	736	15312
Azk	1769	1283	17613